

Fully-gapped superconductivity with preserved time-reversal symmetry in NiBi₃ single crystals

T. Shang,^{1,2,*} J. Meng,¹ X. Y. Zhu,¹ H. Zhang,¹ B. C. Yu,¹ Z. X. Zhen,¹
Y. H. Wang,¹ Y. Xu,¹ Q. F. Zhan,¹ D. J. Gawryluk,³ and T. Shiroka^{4,5}

¹Key Laboratory of Polar Materials and Devices (MOE), School of Physics and Electronic Science, East China Normal University, Shanghai 200241, China

²Chongqing Key Laboratory of Precision Optics, Chongqing Institute of East China Normal University, Chongqing 401120, China

³Laboratory for Multiscale Materials Experiments, Paul Scherrer Institut, CH-5232 Villigen PSI, Switzerland

⁴Laboratory for Muon-Spin Spectroscopy, Paul Scherrer Institut, CH-5232 Villigen PSI, Switzerland

⁵Laboratorium für Festkörperphysik, ETH Zürich, CH-8093 Zürich, Switzerland

We report a study of NiBi₃ single crystals by means of electrical-resistivity-, magnetization-, and muon-spin rotation and relaxation (μ SR) measurements. As a single crystal, NiBi₃ adopts a needle-like shape and exhibits bulk superconductivity with $T_c \approx 4.1$ K. By applying magnetic fields parallel and perpendicular to the b -axis of NiBi₃, we establish that its lower- and upper critical fields, as well as the magnetic penetration depths show slightly different values, suggesting a weakly anisotropic superconductivity. In both cases, the zero-temperature upper critical fields are much smaller than the Pauli-limit value, indicating that the superconducting state is constrained by the orbital pair breaking. The temperature evolution of the superfluid density, obtained from transverse-field μ SR, reveals a fully-gapped superconductivity in NiBi₃, with a shared superconducting gap $\Delta_0 = 2.1 k_B T_c$ and magnetic penetration depths $\lambda_0 = 223$ and 210 nm for $H \parallel b$ - and $H \perp b$, respectively. The lack of spontaneous fields below T_c indicates that time-reversal symmetry is preserved in NiBi₃. The absence of a fast muon-spin relaxation and/or precession in the zero-field μ SR spectra definitely rules out any type of magnetic ordering in NiBi₃ single crystals. Overall, our investigation suggests that NiBi₃ behaves as a conventional s -type superconductor.

I. INTRODUCTION

Topological superconductors offer many attractive properties, which range from the possibility to host Majorana quasiparticles to enabling topological quantum computing [1–3]. This has spurred researchers to explore different routes and/or materials to realize them. For instance, superconductors with $p + ip$ pairing have been predicted to support Majorana bound states at their vortices [4]. Besides relying on bulk superconductors with nontrivial electronic bands, another approach towards topological superconductivity (SC) consists in combining conventional s -wave superconductors with topological insulators or ferromagnets, so as to form heterostructures. In both cases, proximity effects at the interface may lead to a two-dimensional superconducting state with an unconventional pairing [5–7].

Among the different types of heterostructures, epitaxial Bi/Ni bilayers have been proposed as a promising candidate for hosting chiral p -wave SC [8]. In fact, tunneling experiments in such bilayers have shown the coexistence of ferromagnetism (FM) and SC below the superconducting transition, at $T_c \approx 4$ K [9]. More recently, surface magneto-optic Kerr-effect measurements revealed spontaneous magnetic fields occurring below the onset of SC, which suggest the breaking of time-reversal symmetry (TRS) in the superconducting state of Bi/Ni bilayers [10]. Finally, time-domain terahertz spectroscopy experiments found a nodeless SC state in Bi/Ni bilayers [11], more consistent with a chiral p -wave SC [12].

At the same time, there is mounting evidence that the occurrence of SC in Bi/Ni bilayers could be related to the formation of a superconducting NiBi₃ phase (with $T_c \approx 4$ K [13–15]) during the thin-film growth [16–23]. This because NiBi₃-free Bi/Ni bilayers show no signs of superconductivity [20, 21]. These observations have triggered the

researchers' interests to study the superconducting properties of pure NiBi₃. Similar to the Bi/Ni bilayers [9], also bulk NiBi₃ shows the coexistence of SC and FM [24–27]. Thus, magnetization data in its superconducting state, show a clear loop of ferromagnetic hysteresis [15, 25, 26]. Generally, superconductivity and ferromagnetism are antagonistic ground states. However, akin to certain U-based materials [28–30], NiBi₃, too, belongs to the rare class of ferromagnetic superconductors, potentially able to host spin-triplet pairing.

To date, the superconducting properties of NiBi₃ have been mostly investigated via magnetic- and transport measurements [13–15, 24–27]. Yet, the microscopic nature of its SC, in particular, the superconducting order parameter, has not been explored and awaits further investigation. In addition, it is not yet clear if the observed breaking of TRS and the unconventional SC of epitaxial Bi/Ni bilayers can be attributed to the formation of the NiBi₃ phase or not [10].

To clarify the above issues, we synthesized NiBi₃ single crystals using the flux method, and studied their superconducting properties by means of electrical-resistivity-, magnetization-, and muon-spin rotation and relaxation (μ SR) measurements. We found that NiBi₃ exhibits a fully-gapped superconducting state with a preserved TRS. The absence of any magnetic order, on the surface or in the bulk of NiBi₃ single crystals, was also confirmed. Our results suggest that NiBi₃ behaves as a conventional s -type superconductor and, thus, the unconventional superconducting properties observed in Bi/Ni bilayers cannot be attributed to the NiBi₃ phase.

II. EXPERIMENTAL DETAILS

The NiBi₃ single crystals were grown from molten bismuth flux. High-purity Bi pieces (Alfa Aesar, 99.99%) and Ni powders (Alfa Aesar, 99.9%) with a 10:1 ratio were loaded in an Al₂O₃ crucible, which was sealed in a quartz ampoule under high vacuum. The quartz ampoule was heated up to 1050 °C and then kept at this temperature for over 24 hours. Finally,

* Corresponding authors:
tshang@phy.ecnu.edu.cn

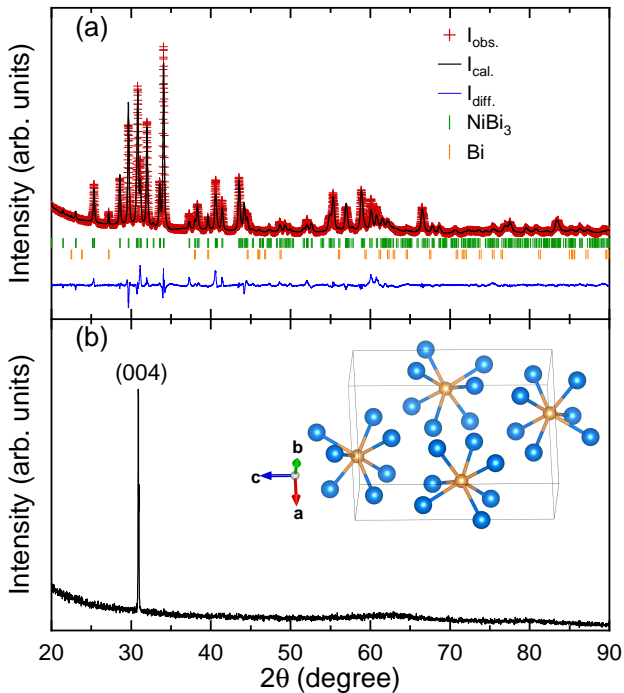


FIG. 1. (a) Room-temperature x-ray powder diffraction pattern and Rietveld refinement for NiBi_3 . The red crosses and the solid black line represent the experimental pattern and the Rietveld refinement profile, respectively. The blue line at the bottom shows the residuals, i.e., the difference between the calculated and experimental data. The vertical bars mark the calculated Bragg-peak positions for NiBi_3 (green) and Bi (orange). The refinement R -factors are $R_p \sim 3.71\%$, $R_{wp} \sim 5.82\%$, and $R_{exp} \sim 1.37\%$. Note that, the minority Bi phase comes from the remaining flux on the surface of crystals. (b) XRD pattern of a NiBi_3 single crystal. The unit cell is shown in the inset, with the blue and orange spheres depicting the Bi and Ni atoms.

it was slowly cooled down to 360°C at a rate of $2^\circ\text{C}/\text{h}$, with the remaining Bi flux being removed via centrifugation. The typical dimensions of the obtained needle-like single crystals were about $\sim 3\text{ mm} \times 0.3\text{ mm} \times 0.3\text{ mm}$ (see below). The crystals were checked by powder x-ray diffraction (XRD), recorded using a Bruker D8 diffractometer. Further characterization involved electrical-resistivity- and magnetization measurements, performed on a Quantum Design physical property measurement system (PPMS) and a magnetic property measurement system (MPMS), respectively. For the electrical-resistivity measurements, the dc current was applied along the b -axis.

The bulk μSR measurements were carried out at the multipurpose surface-muon spectrometer (Dolly) on the πE1 beamline of the Swiss muon source at Paul Scherrer Institut, Villigen, Switzerland. The crystals were aligned and mounted on a $25\text{-}\mu\text{m}$ thick copper foil, which ensured thermalization at low temperatures. The magnetic fields were applied both parallel and perpendicular to the b -axis of the NiBi_3 single crystal. The time-differential μSR data were collected upon heating and then analyzed by means of the `musrfit` software package [31].

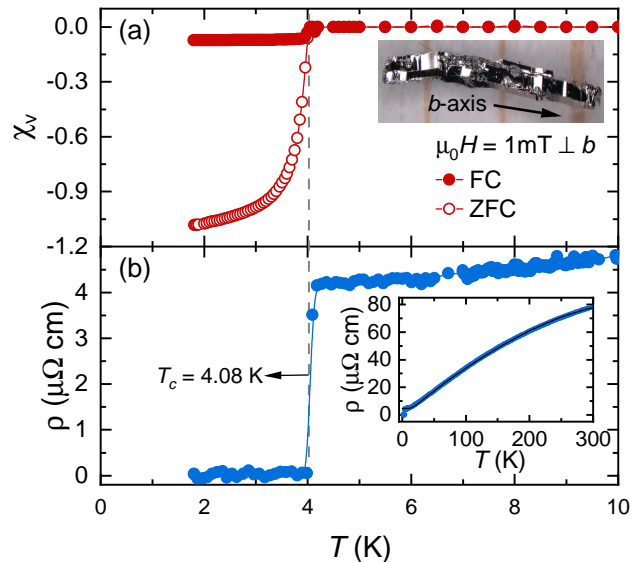


FIG. 2. Temperature-dependent magnetic susceptibility $\chi_V(T)$ (a) and electrical resistivity $\rho(T)$ (b) for a NiBi_3 single crystal. The dashed lines mark the T_c value. While $\rho(T)$ was measured in zero-field conditions, $\chi_V(T)$ data were collected in a magnetic field of 1 mT , applied perpendicular to the b -axis. The susceptibility data were corrected to account for the demagnetization factor. The upper inset depicts a needle-like NiBi_3 single crystal, with the arrow indicating the b -axis, while the lower inset shows $\rho(T)$ up to 300 K . In the latter case, the solid black line is a fit to the equation discussed in the text.

III. RESULTS AND DISCUSSION

A. Crystal structure

The crystal structure and phase purity of NiBi_3 single crystals were checked via XRD at room temperature. As shown in Fig. 1, we performed Rietveld refinements of the XRD pattern by using the Fullprof suite [32]. Consistent with previous results, we confirm that NiBi_3 crystallizes in a centrosymmetric orthorhombic structure with a space group $Pnma$ (No. 62) [13–15, 24–27]. In this structure, bismuth atoms form an octahedral array, while nickel atoms form part of linear chains [25]. The crystal structure of a unit cell is shown in the inset of Fig. 1(b). The refined lattice parameters, $a = 8.8799(1)\text{ \AA}$, $b = 4.09831(6)\text{ \AA}$, and $c = 11.4853(1)\text{ \AA}$, are in good agreement with the results reported in the literature [13–15, 24–27]. According to the refinements in Fig. 1, a tiny amount of elemental bismuth ($\sim 1\%$) was also identified, here attributed to the remanent Bi-flux on the surface of single crystals. Considering its small amount and the fact that Bi is not superconducting in the studied temperature range [33], the bismuth presence has negligible effects on the superconducting properties of NiBi_3 . We also performed XRD measurement on a NiBi_3 single crystal. As shown in Fig. 1(b), only the (004) reflection [the strongest among the (00 l)-reflections] was detected, confirming the single-crystal nature of the NiBi_3 sample.

B. Bulk superconductivity

The bulk superconductivity of NiBi_3 single crystals was first characterized by magnetic-susceptibility measurements,

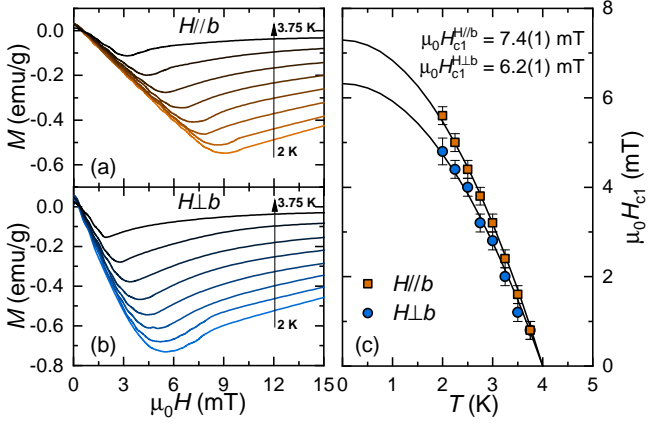


FIG. 3. Field-dependent magnetization curves collected at various temperatures after cooling the NiBi₃ single crystal in zero field for (a) $H \parallel b$ and (b) $H \perp b$. (c) The respective lower critical fields H_{c1} vs. temperature. Solid lines are fits to $\mu_0 H_{c1}(T) = \mu_0 H_{c1}(0)[1 - (T/T_c)^2]$. For each temperature, H_{c1} was determined as the value where $M(H)$ starts deviating from linearity. The lower critical fields were corrected by a demagnetization factor N , which is 0.5 for $H \perp b$. Since the NiBi₃ crystal is needle-like, no demagnetization factor is required for $H \parallel b$ (i.e., $N = 0$).

using both field-cooling (FC) and zero-field-cooling (ZFC) protocols in an applied field of 1 mT. As shown in Fig. 2(a), a clear diamagnetic response appears below the superconducting transition at $T_c = 4.05$ K. Similar results were obtained when applying the magnetic field parallel to the b -axis. After accounting for the demagnetization factor N , which is estimated to be 0.5 for $H \perp b$ and 0 for $H \parallel b$ [34], the superconducting shielding fraction of NiBi₃ was found to be close to 100%, indicative of bulk SC.

The temperature-dependent electrical resistivity $\rho(T)$ of NiBi₃ single crystals was measured from 2 K up to room temperature. It reveals a metallic behavior, without any anomalies associated with phase transitions in the normal state [see inset in Fig. 2(b)]. The electrical resistivity in the low-temperature region is plotted in the main panel of Fig. 2(b), where the superconducting transition (with $T_c^{\text{onset}} = 4.16$ K, $T_c^{\text{mid}} = 4.08$ K and $T_c^{\text{zero}} = 4.0$ K) is clearly seen. As shown by the dashed-line in Fig. 2, the T_c^{mid} value is consistent with the onset of the superconducting transition in the magnetic susceptibility. Therefore, the T_c^{mid} values were used to determine the upper critical field of NiBi₃. The $\rho(T)$ curve can be described by the Bloch-Grüneisen-Mott (BGM) formula

$$\rho(T) = \rho_0 + 4A \left(\frac{T}{\Theta_D^R} \right)^5 \int_0^{\frac{\Theta_D^R}{T}} \frac{z^2 dz}{(e^z - 1)(1 - e^{-z})} - \alpha T^3$$
 [35, 36]. Here, the first term ρ_0 is the residual resistivity due to the scattering of conduction electrons on the static defects of the crystal lattice, while the second term describes the electron-phonon scattering, with Θ_D^R being the characteristic (Debye) temperature and A a coupling constant. The third term represents a contribution due to s - d interband scattering, α being the Mott coefficient [37, 38]. The fit in Fig. 2 (solid black line) results in $\rho_0 = 4.5(2) \mu\Omega\text{cm}$, $A = 32(1) \mu\Omega\text{cm}$, $\Theta_D^R = 100(3)$ K, and $\alpha = 8.0(2) \times 10^{-7} \mu\Omega\text{cmK}^{-3}$. The derived Θ_D^R is comparable with the value determined from low- T specific heat [13]. The fairly large residual resistivity ratio (RRR), i.e., $\rho(300 \text{ K})/\rho_0 \sim 18$, and the sharp superconducting transition ($\Delta T_c = 0.15$ K) both indicate a good sample quality.

C. Lower and upper critical fields

To determine the lower critical field H_{c1} , the field-dependent magnetization $M(H)$ of a NiBi₃ single crystal was measured at various temperatures up to 3.75 K. Figure 3(a)-(b) plots the $M(H)$ for $H \parallel b$ and $H \perp b$, respectively. The estimated H_{c1} values at different temperatures (accounting for a demagnetization factor) are summarized in Fig. 3(c). The solid lines are fits to $\mu_0 H_{c1}(T) = \mu_0 H_{c1}(0)[1 - (T/T_c)^2]$ and yield the lower critical fields $\mu_0 H_{c1}(0) = 7.4(1)$ and $6.2(1)$ mT for $H \parallel b$ and $H \perp b$, respectively. The zero-temperature $H_{c1}^{H \parallel b}/H_{c1}^{H \perp b}$ ratio (~ 1.2) suggests a weakly anisotropic superconductivity in the NiBi₃ single crystal.

We also performed temperature-dependent electrical-resistivity measurements $\rho(T, H)$ at various applied magnetic fields, as well as studied the field-dependent magnetization $M(H, T)$ at various temperatures by applying the magnetic field either parallel or perpendicular to the b -axis of the NiBi₃ single crystal. As shown in Fig. 4(a), upon increasing the magnetic field, the superconducting transition in $\rho(T)$ shifts to lower temperatures. Similarly, in the $M(H)$ data, the diamagnetic signal vanishes once the applied magnetic field exceeds the upper critical field H_{c2} . For $H \parallel b$, no zero resistivity is observed down to ~ 2 K for $\mu_0 H > 0.35$ T. For $H \perp b$, the zero resistivity already vanishes for $\mu_0 H > 0.25$ T, implying that, in NiBi₃, the H_{c2} value along the b -axis is larger than that perpendicular to it.

Figure 4(e) and (f) summarizes the upper critical fields H_{c2} vs. the reduced superconducting transition temperature $T_c/T_c(0)$ for both $H \parallel b$ and $H \perp b$, as identified from the $\rho(T, H)$ and $M(H, T)$ data. The temperature evolution of the upper critical field $H_{c2}(T)$ is well described by the Werthamer-Helfand-Hohenberg (WHH) model [39]. As shown by the dash-dotted lines in Fig. 4(e)-(f), the WHH model agrees remarkably well with the experimental data and provides $\mu_0 H_{c2}^{H \parallel b}(0) = 0.70(2)$ T and $\mu_0 H_{c2}^{H \perp b}(0) = 0.41(1)$, respectively. These values are comparable to previous results [13, 15, 27] and both are much smaller than the Pauli-limiting field (i.e., $1.86T_c \sim 7.4$ T). Consequently, the orbital pair-breaking mechanism seems to be dominant in NiBi₃. Similarly to the lower critical fields, also the $H_{c2}^{H \parallel b}/H_{c2}^{H \perp b}$ ratio (~ 1.7) confirms the weakly anisotropic SC in NiBi₃.

In the Ginzburg-Landau (GL) theory of superconductivity, the magnetic penetration depth λ is related to the coherence length ξ , and the lower critical field via $\mu_0 H_{c1} = (\Phi_0/4\pi\lambda^2)\ln(\kappa)$, where $\Phi_0 = 2.07 \times 10^3$ T nm² is the quantum of magnetic flux, $\kappa = \lambda/\xi$ is the GL parameter [40]. By using $\mu_0 H_{c1}$ and ξ values [calculated from $\mu_0 H_{c2}(0) = \Phi_0/2\pi\xi(0)^2$], the resulting $\lambda_{\text{GL}}(0) = 229(2)$ and $238(2)$ nm for $H \parallel b$ and $H \perp b$ are both compatible with the experimental value determined from μSR data. All the superconducting parameters are summarized in Table I.

D. TF- μSR and fully-gapped superconductivity

To investigate the single-crystal anisotropy of superconducting pairing in NiBi₃, we carried out systematic transverse-field (TF-) μSR measurements, where we applied the field along different orientations. Representative TF- μSR spectra collected in a field of 14.5 mT in the superconducting- and normal states of NiBi₃ are shown in Fig. 5(a) for $H \parallel b$ -

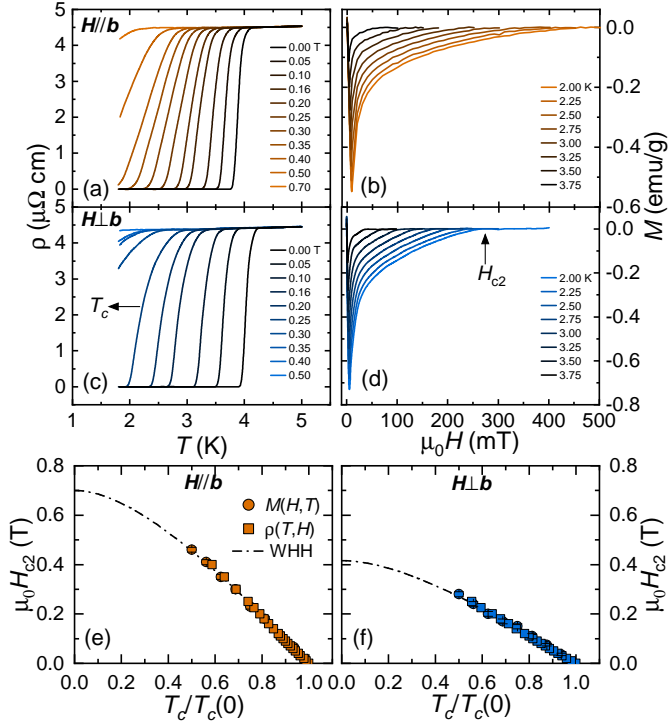


FIG. 4. Temperature-dependent electrical resistivity $\rho(T, H)$ for various applied magnetic fields (a) and field-dependent magnetization curves $M(H, T)$, collected at various temperatures below T_c (b), for the $H \parallel b$ case. The analogue results for $H \perp b$ are shown in panels (c) and (d). In $\rho(T, H)$, T_c was chosen as the mid-point of the superconducting transition (see details in Fig. 2). While in $M(H, T)$, H_{c2} was determined as the field where the diamagnetic response vanishes (here indicated by an arrow). Upper critical field H_{c2} vs. the reduced transition temperature $T_c/T_c(0)$ for $H \parallel b$ (e) and $H \perp b$ (f), respectively. The T_c and H_{c2} values were determined from the measurements shown in panels (a)-(d). Circles refer to magnetization, while squares refer to resistivity measurements. The dash-dotted lines represent fits to the WHH model.

axis and in Fig. 5(b) for $H \perp b$ -axis. In the latter case, the TF- μ SR spectra were also collected in a field of 30 mT [see Fig. 5(c)]. In case of a type-II superconductor (see, e.g., the 0.3-K data in Fig. 5), the development of a flux-line lattice (FLL) causes an inhomogeneous field distribution and, thus, it gives rise to an additional damping in the TF- μ SR spectra [41]. These are generally modeled using [42]:

$$A_{\text{TF}}(t) = \sum_{i=1}^n A_i \cos(\gamma_{\mu} B_i t + \phi) e^{-\sigma_i^2 t^2 / 2} + A_{\text{bg}} \cos(\gamma_{\mu} B_{\text{bg}} t + \phi). \quad (1)$$

Here A_i ($\sim 85\%$), A_{bg} ($\sim 15\%$) and B_i , B_{bg} are the initial asymmetries and local fields sensed by the implanted muons in the sample and sample holder (i.e., Cu) or in the residual bismuth, $\gamma_{\mu}/2\pi = 135.53$ MHz/T is the muon gyromagnetic ratio, ϕ is a shared initial phase, and σ_i is the Gaussian relaxation rate of the i th component. Note that, in the studied temperature range, the effects of the residual bismuth are negligible due to its non-magnetic and non-superconducting nature. We find that two oscillations (i.e., $n = 2$) are required to describe the TF- μ SR spectra for both $H \parallel b$ - and $H \perp b$ -axis (see solid lines in Fig. 5). Indeed, as shown in Fig. 5(a)-(c), oscillations with two distinct frequencies can be clearly identified and, generally, the model with two oscillations provides a better fit than that with a single oscillation.

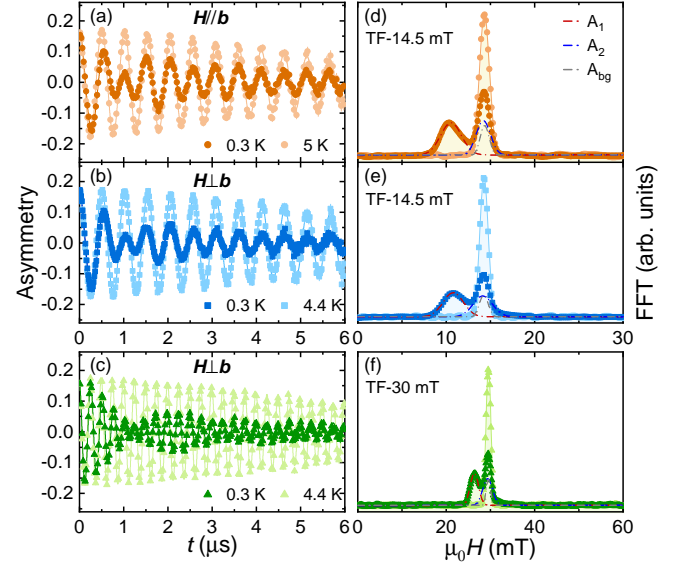


FIG. 5. TF- μ SR spectra in the normal- and superconducting states of NiBi₃ single crystals in an applied magnetic field of 14.5 mT for $H \parallel b$ (a) and $H \perp b$ (b), respectively. The fast Fourier transforms of the TF- μ SR spectra in panels (a) and (b) are shown in panels (d) and (e), respectively. For $H \perp b$ -axis, the TF- μ SR and FFT spectra for an applied magnetic field of 30 mT are shown in panels (c) and (f), respectively. Solid lines are fits to Eq. (1) using two oscillations, here also shown separately as dash-dotted lines in (c)-(f), together with a background contribution. Note the clear field-distribution broadening due to the onset of FLL below T_c .

For example, in Fig. 5(c), the two-oscillation model yields a goodness-of-fit parameter $\chi_r^2 \sim 1.4$, twice smaller than the single-oscillation fit ($\chi_r^2 \sim 3.2$). The fast Fourier transforms (FFT) of the TF- μ SR spectra at 0.3 K are shown by dash-dotted lines in Fig. 5(d)-(f), which illustrate the two components (A_1 and A_2) and the background signal (A_{bg}). The two-peak FFT in NiBi₃ might be related to two different muon-stopping sites, a feature to be confirmed by future DFT calculations.

The derived muon-spin relaxation rates σ_i are small and temperature-independent in the normal state, but below T_c they start to increase due to the onset of FLL and the increased superfluid density. At the same time, a diamagnetic field shift, $\Delta B(T) = \langle B \rangle - B_{\text{appl}}$, appears below T_c , with $\langle B \rangle = (A_1 B_1 + A_2 B_2)/A_{\text{tot}}$, where $A_{\text{tot}} = A_1 + A_2$ and B_{appl} is the applied external field (see, e.g., the inset of Fig. 6). The effective Gaussian relaxation rate can be calculated from $\sigma_{\text{eff}}^2/\gamma_{\mu}^2 = \sum_{i=1}^2 A_i [\sigma_i^2/\gamma_{\mu}^2 - (B_i - \langle B \rangle)^2]/A_{\text{tot}}$ [42]. Then, the superconducting Gaussian relaxation rate σ_{sc} can be extracted by subtracting the nuclear contribution according to $\sigma_{\text{sc}} = \sqrt{\sigma_{\text{eff}}^2 - \sigma_n^2}$. Here, σ_n is the nuclear relaxation rate, almost constant in the covered temperature range and relatively small in NiBi₃, as confirmed also by the ZF- μ SR data (see Fig. 7). Since the applied TF fields (14.5 and 30 mT) are not really small compared to the modest upper critical fields of NiBi₃ [see Fig. 4(e) and (f)], to calculate the magnetic penetration depth λ from σ_{sc} we had to consider the overlap of the vortex cores. Consequently, in our case, λ was calculated by means of $\sigma_{\text{sc}} = 0.172 \frac{\gamma_{\mu} \Phi_0}{2\pi} (1-h)[1 + 1.21(1-\sqrt{h})^3] \lambda^{-2}$, where $h = B_{\text{appl}}/B_{c2}$ [43, 44].

Figure 6 summarizes the temperature-dependent inverse square of the magnetic penetration depth [proportional to the superfluid density, i.e., $\lambda^{-2}(T) \propto \rho_{\text{sc}}(T)$] for both $H \parallel b$

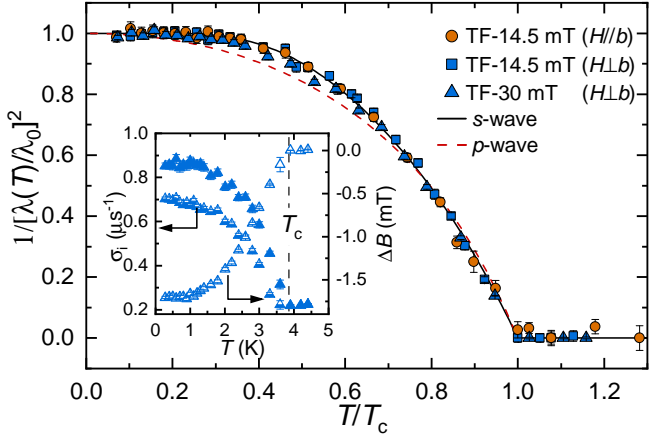


FIG. 6. Superfluid density vs. reduced temperature T/T_c for NiBi_3 single crystals. Inset shows the temperature-dependent muon-spin relaxation rate $\sigma_i(T)$ (left axis) and the diamagnetic shift $\Delta B(T)$ (right-axis) for the TF-30 mT- μSR spectra. The solid line in the main panel represents a fit to the fully gapped s -wave model with a single energy gap, while the dashed line is a fit using the p -wave model to the $H \parallel b$ -data.

and $H \perp b$. For $H \perp b$, the data collected in a field of 30 mT are also presented. The $\rho_{\text{sc}}(T)$ was analyzed by applying different models, generally described by:

$$\rho_{\text{sc}}(T) = 1 + 2 \left\langle \int_{\Delta_{\mathbf{k}}}^{\infty} \frac{E}{\sqrt{E^2 - \Delta_{\mathbf{k}}^2}} \frac{\partial f}{\partial E} dE \right\rangle_{\text{FS}}. \quad (2)$$

Here, $f = (1 + e^{E/k_B T})^{-1}$ is the Fermi function [40]; $\Delta_{\mathbf{k}}(T) = \Delta(T)\delta_{\mathbf{k}}$ is an angle-dependent gap function, where Δ is the maximum gap value and $\delta_{\mathbf{k}}$ is the angular dependence of the gap, equal to 1 and $\sin\theta$ for an s - and p -wave model, respectively, with θ being the azimuthal angles. The temperature dependence of the gap is assumed to follow $\Delta(T) = \Delta_0 \tanh\{1.82[1.018(T_c/T - 1)]^{0.51}\}$ [40, 45], where Δ_0 is the gap value at 0 K. As can be clearly seen in Fig. 6 (see dashed line), the p -wave model exhibits a significant deviation from the experimental data. While the temperature-invariant superfluid density below $T_c/3$ strongly suggests the absence of low-energy excitations and, hence, a fully-gapped superconducting state in NiBi_3 . Consequently, the $\rho_{\text{sc}}(T)$ is more consistent with the s -wave model. As shown by the solid line in Fig. 6, in both cases (i.e., $H \parallel b$ - and $H \perp b$ -axis), the s -wave model describes $\rho_{\text{sc}}(T)$ very well across the entire temperature range and yields a zero-temperature gap $\Delta_0 = 2.10(5) k_B T_c$. Such isotropic gap value along different crystal directions is consistent with previous Andreev-reflection spectroscopy results [46]. For $H \parallel b$, the estimated λ_0^{ac} is 223(2) nm, while for $H \perp b$, we find $\lambda_0^{\text{b}} = 216(2)$ and 210(2) nm for TF-14.5 mT and TF-30 mT, respectively. The small $\lambda_0^{\text{ac}}/\lambda_0^{\text{b}}$ ratio (here, ~ 1.03) and the similar gap sizes along different crystal directions confirm once more the weakly anisotropic SC of NiBi_3 single crystals. Note that, although the single-oscillation model also gives a temperature-independent superfluid density below $1/3T_c$ as the two-oscillation model, the estimated λ_0 values by using the former model are significantly different from the values estimated from the magnetization data.

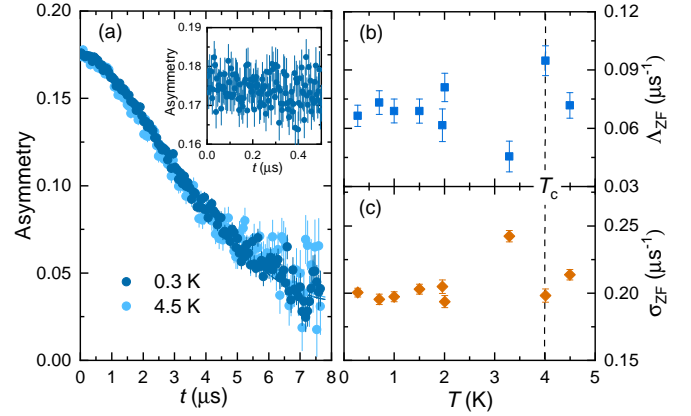


FIG. 7. Representative ZF- μSR spectra of a NiBi_3 single crystal in the superconducting- (0.3 K) and in the normal states (4.5 K) (a). The inset shows an enlarged plot of 0.3 K-ZF- μSR on a short time scale. Solid lines are fits to the equation described in the text, with the derived temperature-dependent Lorentzian- $\Lambda_{\text{ZF}}(T)$ and Gaussian $\sigma_{\text{ZF}}(T)$ relaxation rates being shown in panels (b) and (c), respectively. The dashed line at 4 K marks the bulk T_c and serves as a guide to the eyes. None of the reported fit parameters shows a distinct enhancement below T_c , thus suggesting a preserved TRS.

E. ZF- μSR and preserved time-reversal symmetry

To search for possible ferromagnetism and breaking of the time-reversal symmetry in a NiBi_3 single crystal, we performed zero-field (ZF-) μSR measurements covering both the normal- and superconducting states. As shown in Fig. 7, neither coherent oscillations nor fast decays could be identified in the spectra collected above- (4.5 K) and below T_c (0.3 K), hence implying the lack of any magnetic order or fluctuations. As clearly demonstrated in the inset of Fig. 7(a), the ZF- μSR spectra are almost flat on a short time scale (i.e., $t < 0.5 \mu\text{s}$), confirming again the absence of fast oscillations which would be caused by a possible ferromagnetic ordering, as instead reported in previous work [24, 25]. Thus, in the absence of external fields, the muon-spin relaxation in NiBi_3 is mainly due to the randomly oriented nuclear moments, which can be modeled by a Gaussian Kubo-Toyabe relaxation function $G_{\text{KT}} = [\frac{1}{3} + \frac{2}{3}(1 - \sigma_{\text{ZF}}^2 t^2) e^{-\sigma_{\text{ZF}}^2 t^2/2}]$ [41, 47]. Here, σ_{ZF} is the zero-field Gaussian relaxation rate. The ZF- μSR spectra were fitted by considering also an additional electronic contribution. The solid lines in Fig. 7(a) represent fits to $A_{\text{ZF}}(t) = A_s G_{\text{KT}} e^{-\Lambda_{\text{ZF}} t} + A_{\text{bg}}$, where Λ_{ZF} is the zero-field exponential muon-spin relaxation rate, A_s and A_{bg} are the same as in TF- μSR [see Eq. (1)]. The derived Λ_{ZF} and σ_{ZF} values as a function of temperature are shown in Fig. 7(b) and (c), respectively. Neither $\Lambda_{\text{ZF}}(T)$ nor $\sigma_{\text{ZF}}(T)$ show a systematic enhancement below T_c . Here, the jump of σ_{ZF} at 3.5 K [Fig. 7(c)] is not related to a TRS-breaking effect, but to the correlated decrease of Λ_{ZF} [Fig. 7(b)]. The lack of an additional relaxation below T_c excludes a possible TRS-breaking effect in the superconducting state of the NiBi_3 single crystal, here also reflected in the practically overlapping datasets shown in Fig. 7(a).

IV. DISCUSSION

First, we discuss the absence of ferromagnetism in NiBi_3 . Previous works found evidence for either extrinsic or intrinsic

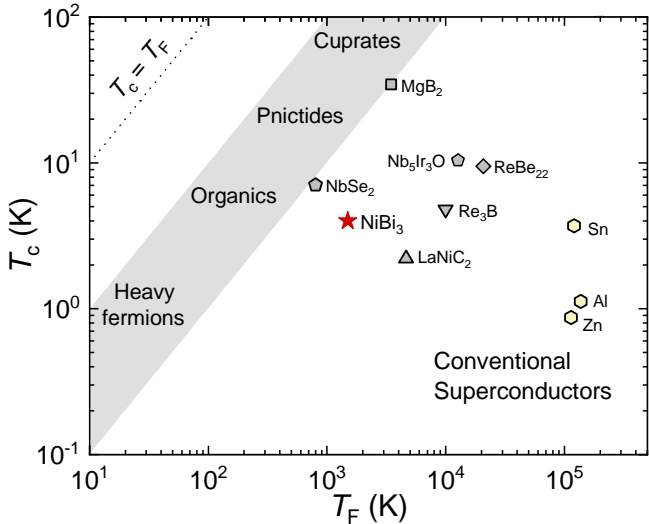


FIG. 8. Uemura plot showing the superconducting transition T_c against the effective Fermi temperature T_F for different kinds of superconductors. The grey region $1/100 < T_c/T_F < 1/10$ delimits the band of unconventional superconductors, including heavy fermions, organics, fullerenes, pnictides, and high- T_c cuprates. A few selected superconductors (see Refs. 48–52) are shown here with different symbols. The dotted line corresponds to $T_c = T_F$, where T_F is the temperature associated with the Fermi energy, $E_F = k_B T_F$.

insic ferromagnetism in NiBi_3 single crystals. In the extrinsic case, the amorphous Ni impurities in NiBi_3 lead to a clear drop in magnetization at temperatures close to their Curie temperature [15]. In NiBi_3 , such FM can even coexist with SC, as demonstrated by the ferromagnetic hysteresis loops observed in the magnetization data [24–26]. Besides bulk crystals with Ni impurities, also submicrometer-sized NiBi_3 particles, or quasi-one-dimensional nanoscale strips of NiBi_3 undergo a ferromagnetic order [26]. In addition, below 150 K, electron-spin-resonance data reveal ferromagnetic-like fluctuations on the surface of NiBi_3 crystals [27]. The above evidence suggests that NiBi_3 is a possible ferromagnetic superconductor, which might enable spin-triplet SC pairing, analogous to that found in other ferromagnetic superconductors [28–30]. Here, we applied the ZF- μ SR technique to detect a possible ferromagnetic order in NiBi_3 single crystals. Due to their large magnetic moment, muons represent one of the most sensitive magnetic probes, able to sense very low internal fields ($\sim 10^{-2}$ mT), and thus, to detect local magnetic fields of either nuclear or electronic origin [41, 53]. In contrast to previous studies, our ZF- μ SR results do not evidence any ferromagnetic order or fluctuations in NiBi_3 , thus implying that the previously reported ferromagnetism is most likely of extrinsic nature. In addition, our ZF- μ SR results indicate that time-reversal symmetry is preserved in the superconducting state of NiBi_3 . This conclusion is further supported by recent high-resolution surface magneto-optic Kerr effect measurements in NiBi_3 single crystals, which also do not find any traces of a spontaneous Kerr signal in the superconducting state [54].

Second, we discuss the weakly anisotropic superconductivity in NiBi_3 . Although NiBi_3 single crystals exhibit a quasi-one dimensional needle-like shape [see inset in Fig. 2(a)], their crystal structure is definitely three dimensional, with $a = 8.8799 \text{ \AA}$, $b = 4.09831 \text{ \AA}$, and $c = 11.4853 \text{ \AA}$ (see Fig. 1).

Such an intrinsically three-dimensional structure could naturally explain the almost isotropic- (or weakly anisotropic) electronic properties of NiBi_3 . As confirmed by our study, the lower critical field H_{c1} (Fig. 3), the upper critical field H_{c2} (Fig. 4), the magnetic penetration depth λ , and the superconducting gap Δ_0 (Fig. 6), all show comparable values for $H \parallel b$ - and $H \perp b$ -axis. These results clearly indicate a weakly anisotropic SC in NiBi_3 single crystals, as also observed in NiBi_3 thin films [18]. Moreover, electrical-resistivity measurements reveal almost identical upper critical fields when the magnetic field is rotated in the ac -plane of a NiBi_3 single crystal [13]. Future electronic band-structure calculations could provide further hints about the observed weak anisotropy.

Finally, let us compare the superconducting parameters of NiBi_3 with those of other superconductors. By using the SC parameters obtained from the measurements presented here, we calculate an effective Fermi temperature $T_F \sim 1.5 \times 10^3 \text{ K}$ for NiBi_3 (here, we consider the $H \parallel b$ case). We recall that T_F is proportional to $n_s^{2/3}/m^*$, where n_s and m^* are the carrier density and the effective mass. The estimated $m^* \sim 8 m_e$, indicates a moderate degree of electronic correlations in NiBi_3 . Different families of superconductors can be classified according to their T_c/T_F ratios into a so-called Uemura plot [49]. In such plot, many conventional superconductors, as e.g., Al, Sn, and Zn, are located at $T_c/T_F < \sim 10^{-4}$. Conversely, several types of unconventional superconductors, including heavy fermions, organics, high- T_c iron pnictides, and cuprates, all lie in the $10^{-2} < T_c/T_F < 10^{-1}$ band. Between these two categories lie a few different types of superconductors, including multigap- and noncentrosymmetric superconductors, etc. [48–52]. Although located clearly far off the conventional band, our TF- and ZF- μ SR results suggest that the NiBi_3 superconductivity is more consistent with a conventional fully-gapped SC with preserved time-reversal symmetry. Such conclusion is also supported by the linear suppression of T_c under applied pressure. For instance, the T_c of NiBi_3 decreases from 4 K to 3 K when the pressure increases from 0 to 2.2 GPa [55].

Table I. Superconducting parameters of NiBi_3 single crystal, as determined from electrical-resistivity, magnetization, and TF-14.5 mT- μ SR measurements.

Property	Unit	$H \parallel b$	$H \perp b$
T_c^x	K	4.05(5)	4.05(5)
$T_c^{\mu\text{SR}}$	K	3.9(1)	3.9(1)
$\mu_0 H_{c1}$	mT	7.4(1)	6.2(1)
$\mu_0 H_{c2}$	T	0.70(1)	0.41(1)
Δ_0 (s-wave)	$k_B T_c$	2.10(5)	2.10(5)
Δ_0 (p-wave)	$k_B T_c$	3.00(5)	3.00(5)
λ_0	nm	223(2)	216(2)
$\xi(0)$	nm	21.7(2)	28.3(3)
$\lambda_{\text{GL}}(0)$	nm	229(2)	238(2)
κ	–	10.5(2)	8.4(2)

V. CONCLUSION

To summarize, we investigated the superconducting properties of flux-grown NiBi_3 single crystals by means of electrical resistivity-, magnetization-, and μ SR measurements. NiBi_3 was shown to exhibit bulk SC with $T_c \sim 4.1 \text{ K}$. By

applying magnetic fields along different crystal directions, we obtained the lower critical field H_{c1} , the upper critical field H_{c2} , and the magnetic penetration depth λ for both the $H \parallel b$ - and $H \perp b$ cases. Both $H_{c2}^{H\parallel b}(0)$ and $H_{c2}^{H\perp b}(0)$ values are much smaller than the Pauli-limit field, implying that the orbital pair-breaking mechanism is dominant in NiBi₃. Although the NiBi₃ single crystals show needle-like shapes, their superconducting properties are only weakly anisotropic, as reflected in the small ratios of $H_{c1}^{H\parallel b}/H_{c1}^{H\perp b}$, $H_{c2}^{H\parallel b}/H_{c2}^{H\perp b}$, and λ_0^a/λ_0^b . The temperature dependence of the NiBi₃ superfluid density reveals a *nodeless* SC, well described by an isotropic *s*-wave model. The relatively large gap value, here, $\Delta_0 = 2.1 k_B T_c$, suggests strong electron-phonon interactions in NiBi₃. Further, the lack of spontaneous magnetic fields below T_c indicates that the time-reversal symmetry is preserved in the NiBi₃ superconductor. The absence of a fast relaxation and/or oscillations in the ZF- μ SR spectra excludes a magnetic order on the surface or in the bulk of NiBi₃ single

crystals, thus implying that the previously observed ferromagnetism is most likely of extrinsic origin. Overall, our systematic results suggest that, in contrast to the unconventional superconductivity observed in Bi/Ni bilayers, NiBi₃ behaves as a conventional *s*-type superconductor.

ACKNOWLEDGMENTS

This work was supported by the Natural Science Foundation of Shanghai (Grants No. 21ZR1420500 and 21JC1402300), Natural Science Foundation of Chongqing (Grant No. 2022NSCQ-MSX1468), and the Schweizerische Nationalfonds zur Förderung der Wissenschaftlichen Forschung (SNF) (Grants No. 200021_188706 and 206021_139082). Y.X. acknowledges support from the Shanghai Pujiang Program (Grant No. 21PJ1403100). We acknowledge the allocation of beam time at the Swiss muon source (Dolly μ SR spectrometer).

-
- [1] X.-L. Qi and S.-C. Zhang, Topological insulators and superconductors, *Rev. Mod. Phys.* **83**, 1057 (2011).
- [2] A. Y. Kitaev, Unpaired Majorana fermions in quantum wires, *Phys. Usp.* **44**, 131 (2001).
- [3] C. Nayak, S. H. Simon, A. Stern, M. Freedman, and S. Das Sarma, Non-abelian anyons and topological quantum computation, *Rev. Mod. Phys.* **80**, 1083 (2008).
- [4] L. Fu and C. L. Kane, Superconducting proximity effect and Majorana fermions at the surface of a topological insulator, *Phys. Rev. Lett.* **100**, 096407 (2008).
- [5] J.-P. Xu, C. Liu, M.-X. Wang, J. Ge, Z.-L. Liu, X. Yang, Y. Chen, Y. Liu, Z.-A. Xu, C.-L. Gao, D. Qian, F.-C. Zhang, and J.-F. Jia, Artificial topological superconductor by the proximity effect, *Phys. Rev. Lett.* **112**, 217001 (2014).
- [6] F. S. Bergeret, A. F. Volkov, and K. B. Efetov, Odd triplet superconductivity and related phenomena in superconductor-ferromagnet structures, *Rev. Mod. Phys.* **77**, 1321 (2005).
- [7] A. I. Buzdin, Proximity effects in superconductor-ferromagnet heterostructures, *Rev. Mod. Phys.* **77**, 935 (2005).
- [8] J. Wang, X. Gong, G. Yang, Z. Lyu, Y. Pang, G. Liu, Z. Ji, J. Fan, X. Jing, C. Yang, F. Qu, X. Jin, and L. Lu, Anomalous magnetic moments as evidence of chiral superconductivity in a Bi/Ni bilayer, *Phys. Rev. B* **96**, 054519 (2017).
- [9] P. LeClair, J. S. Moodera, J. Philip, and D. Heiman, Coexistence of ferromagnetism and superconductivity in Ni/Bi bilayers, *Phys. Rev. Lett.* **94**, 037006 (2005).
- [10] X. Gong, M. Kargarian, A. Stern, D. Yue, H. Zhou, X. Jin, V. M. Galitski, V. M. Yakovenko, and J. Xia, Time-reversal symmetry-breaking superconductivity in epitaxial bismuth/nickel bilayers, *Sci. Adv.* **3**, e1602579 (2017).
- [11] P. Chauhan, F. Mahmood, D. Yue, P.-C. Xu, X. Jin, and N. P. Armitage, Nodeless bulk superconductivity in the time-reversal symmetry breaking Bi/Ni bilayer system, *Phys. Rev. Lett.* **122**, 017002 (2019).
- [12] S.-P. Chao, Superconductivity in a Bi/Ni bilayer, *Phys. Rev. B* **99**, 064504 (2019).
- [13] Y. Fujimori, S.-i. Kan, B. Shinozaki, and T. Kawaguti, Superconducting and normal state properties of NiBi₃, *J. Phys. Soc. Jpn.* **69**, 3017 (2000).
- [14] J. Kumar, A. Kumar, A. Vajpayee, B. Gahtori, D. Sharma, P. K. Ahluwalia, S. Auluck, and V. P. S. Awana, Physical property and electronic structure characterization of bulk superconducting Bi₃Ni, *Supercond. Sci. Technol.* **24**, 085002 (2011).
- [15] B. Silva, R. F. Luccas, N. M. Nemes, J. Hanko, M. R. Osorio, P. Kulkarni, F. Mompean, M. García-Hernández, M. A. Ramos, S. Vieira, and H. Suderow, Superconductivity and magnetism on flux-grown single crystals of NiBi₃, *Phys. Rev. B* **88**, 184508 (2013).
- [16] V. Siva, K. Senapati, B. Satpati, S. Prusty, D. K. Avasthi, D. Kanjilal, and P. K. Sahoo, Spontaneous formation of superconducting NiBi₃ phase in Ni-Bi bilayer films, *J. Appl. Phys.* **117**, 083902 (2015).
- [17] V. Siva, P. C. Pradhan, G. Santosh Babu, M. Nayak, P. K. Sahoo, and K. Senapati, Superconducting proximity effect in NiBi₃-Ni-NiBi₃ trilayer system with sharp superconductor-ferromagnet boundaries, *J. Appl. Phys.* **119**, 063902 (2016).
- [18] W.-L. Wang, Y.-M. Zhang, Y.-F. Lv, H. Ding, L. Wang, W. Li, K. He, C.-L. Song, X.-C. Ma, and Q.-K. Xue, Anisotropic superconductivity and elongated vortices with unusual bound states in quasi-one-dimensional nickel-bismuth compounds, *Phys. Rev. B* **97**, 134524 (2018).
- [19] E. Bhatia, A. Talapatra, J. R. Mohanty, and K. Senapati, Superconductivity, Kondo effect, and observation of self-organized pattern formation in intermetallic NiBi₃ thin films, *Intermetallics* **94**, 160 (2018).
- [20] L. Y. Liu, Y. T. Xing, I. L. C. Merino, H. Micklitz, D. F. Franceschini, E. Baggio-Saitovitch, D. C. Bell, and I. G. Solórzano, Superconductivity in Bi/Ni bilayer system: Clear role of superconducting phases found at Bi/Ni interface, *Phys. Rev. Materials* **2**, 014601 (2018).
- [21] M. Vaughan, N. Satchell, M. Ali, C. J. Kinane, G. B. G. Stenning, S. Langridge, and G. Burnell, Origin of superconductivity at nickel-bismuth interfaces, *Phys. Rev. Res.* **2**, 013270 (2020).
- [22] B. Das, M. Sahoo, A. Patra, A. K. Yadav, S. N. Jha, P. Samal, K. Senapati, and P. K. Sahoo, Phase evolution in thermally annealed Ni/Bi multilayers studied by X-ray absorption spectroscopy, *Phys. Chem. Chem. Phys.* **24**, 4415 (2022).
- [23] M. M. Doria, L. Liu, Y. Xing, I. L. C. Merino, F. J. Litterst, and E. Baggio-Saitovitch, Shape resonances and the T_c dependence on film thickness of Ni/Bi systems, *Supercond. Sci. Technol.* **35**, 015012 (2022).
- [24] L. Liu, Y. Xing, I. L. C. Merino, D. F. Franceschini, I. G. Solórzano, and E. Baggio-Saitovitch, Magnetic properties of superconducting phases NiBi and NiBi₃ formed during pulsed laser deposition of Ni-Bi films, *J. Magn. Magn. Mater.* **514**, 167275 (2020).
- [25] E. L. M. Piñeiro, B. L. R. Herrera, R. Escudero, and L. Bucio, Possible coexistence of superconductivity and magnetism in intermetallic NiBi₃, *Solid State Commun.* **151**, 425 (2011).

- [26] T. Herrmannsdörfer, R. Skrotzki, J. Wosnitza, D. Köhler, R. Boldt, and M. Ruck, Structure-induced coexistence of ferromagnetic and superconducting states of single-phase Bi_3Ni seen via magnetization and resistance measurements, *Phys. Rev. B* **83**, 140501(R) (2011).
- [27] X. Zhu, H. Lei, C. Petrovic, and Y. Zhang, Surface-induced magnetic fluctuations in a single-crystal NiBi_3 superconductor, *Phys. Rev. B* **86**, 024527 (2012).
- [28] S. S. Saxena, P. Agarwal, K. Ahilan, F. M. Grosche, R. K. W. Haselwimmer, M. J. Steiner, E. Pugh, I. R. Walker, S. R. Julian, P. Monthoux, G. G. Lonzarich, A. Huxley, I. Sheikin, D. Braithwaite, and J. Flouquet, Superconductivity on the border of itinerant-electron ferromagnetism in UGe_2 , *Nature* **406**, 587 (2000).
- [29] D. Aoki, A. Huxley, E. Ressouche, D. Braithwaite, J. Flouquet, J.-P. Brison, E. Lhotel, and C. Paulsen, Coexistence of superconductivity and ferromagnetism in URhGe , *Nature* **413**, 613 (2001).
- [30] N. T. Huy, A. Gasparini, D. E. de Nijs, Y. Huang, J. C. P. Klaasse, T. Gortenmulder, A. de Visser, A. Hamann, T. Görlach, and H. v. Löhneysen, Superconductivity on the border of weak itinerant ferromagnetism in UCoGe , *Phys. Rev. Lett.* **99**, 067006 (2007).
- [31] A. Suter and B. M. Wojek, Musrfit: A free platform-independent framework for μSR data analysis, *Phys. Procedia* **30**, 69 (2012).
- [32] J. Rodríguez-Carvajal, Recent advances in magnetic structure determination by neutron powder diffraction, *Physica B: Condens. Matter* **192**, 55 (1993).
- [33] O. Prakash, A. Kumar, A. Thamizhavel, and S. Ramakrishnan, Evidence for bulk superconductivity in pure bismuth single crystals at ambient pressure, *Science* **355**, 52 (2017).
- [34] R. Prozorov and V. G. Kogan, Effective demagnetizing factors of diamagnetic samples of various shapes, *Phys. Rev. Appl.* **10**, 014030 (2018).
- [35] F. Bloch, Zum elektrischen Widerstandsgesetz bei tiefen Temperaturen, *Z. Phys.* **59**, 208 (1930).
- [36] F. J. Blatt, *Physics of Electronic Conduction in Solids* (McGraw-Hill, New York, 1968) p. 185–190.
- [37] N. F. Mott and H. Jones, *The Theory of the Properties of Metals and Alloys* (Oxford University Press, London, 1958).
- [38] N. F. Mott, Electrons in transition metals, *Adv. Phys.* **13**, 325 (1964), p. 403.
- [39] N. R. Werthamer, E. Helfand, and P. C. Hohenberg, Temperature and purity dependence of the superconducting critical field, H_{c2} . III. Electron spin and spin-orbit effects, *Phys. Rev.* **147**, 295 (1966).
- [40] M. Tinkham, *Introduction to Superconductivity*, 2nd ed. (Dover Publications, Mineola, NY, 1996).
- [41] A. Yaouanc and P. D. de Réotier, *Muon Spin Rotation, Relaxation, and Resonance: Applications to Condensed Matter* (Oxford University Press, Oxford, 2011).
- [42] A. Maisuradze, R. Khasanov, A. Shengelaya, and H. Keller, Comparison of different methods for analyzing μSR line shapes in the vortex state of type-II superconductors, *J. Phys.: Condens. Matter* **21**, 075701 (2009), and references therein.
- [43] W. Barford and J. M. F. Gunn, The theory of the measurement of the London penetration depth in uniaxial type-II superconductors by muon spin rotation, *Physica C* **156**, 515 (1988).
- [44] E. H. Brandt, Properties of the ideal Ginzburg-Landau vortex lattice, *Phys. Rev. B* **68**, 054506 (2003).
- [45] A. Carrington and F. Manzano, Magnetic penetration depth of MgB_2 , *Physica C* **385**, 205 (2003).
- [46] G. J. Zhao, X. X. Gong, P. C. Xu, B. C. Li, Z. Y. Huang, X. F. Jin, X. D. Zhu, and T. Y. Chen, Singlet superconductivity in a single-crystal NiBi_3 superconductor, *Supercond. Sci. Technol.* **31**, 125005 (2018).
- [47] R. Kubo and T. Toyabe, A stochastic model for low-field resonance and relaxation, in *Magnetic Resonance and Relaxation. Proceedings of the XIVth Colloque Ampère*, edited by R. Blinc (North-Holland, Amsterdam, 1967) pp. 810–823.
- [48] T. Shang, A. Amon, D. Kasinathan, W. Xie, M. Bobnar, Y. Chen, A. Wang, M. Shi, M. Medarde, H. Q. Yuan, and T. Shiroka, Enhanced T_c and multiband superconductivity in the fully-gapped ReBe_{22} superconductor, *New J. Phys.* **21**, 073034 (2019).
- [49] Y. J. Uemura, L. P. Le, G. M. Luke, B. J. Sternlieb, W. D. Wu, J. H. Brewer, T. M. Riseman, C. L. Seaman, M. B. Maple, M. Ishikawa, D. G. Hinks, J. D. Jorgensen, G. Saito, and H. Yamochi, Basic similarities among cuprate, bismuthate, organic, Chevrel-phase, and heavy-fermion superconductors shown by penetration-depth measurements, *Phys. Rev. Lett.* **66**, 2665 (1991).
- [50] Y. J. Uemura, Twin spin/charge roton mode and superfluid density: Primary determining factors of T_c in high- T_c superconductors observed by neutron, ARPES, and μSR , *Physica B* **374**, 1 (2006).
- [51] Y. Xu, S. Jöhr, L. Das, J. Kitagawa, M. Medarde, T. Shiroka, J. Chang, and T. Shang, Crossover from multiple- to single-gap superconductivity in $\text{Nb}_5\text{Ir}_{3-x}\text{Pt}_x\text{O}$ alloys, *Phys. Rev. B* **101**, 134513 (2020).
- [52] T. Shang, J. Philippe, J. A. T. Verezhak, Z. Guguchia, J. Z. Zhao, L.-J. Chang, M. K. Lee, D. J. Gawryluk, E. Pomjakushina, M. Shi, M. Medarde, H.-R. Ott, and T. Shiroka, Nodeless superconductivity and preserved time-reversal symmetry in the noncentrosymmetric Mo_3P superconductor, *Phys. Rev. B* **99**, 184513 (2019).
- [53] A. Amato, Heavy-fermion systems studied by μSR technique, *Rev. Mod. Phys.* **69**, 1119 (1997).
- [54] J. Wang, C. Farhang, D. Yue, X. Jin, X. Zhu, and J. Xia, Absence of spontaneous time-reversal symmetry breaking and ferromagnetism in superconducting NiBi_3 single crystal, [arXiv:2208.10645 \[cond-mat.supr-con\]](https://arxiv.org/abs/2208.10645) (2022).
- [55] E. Gati, L. Xiang, L.-L. Wang, S. Manni, P. C. Canfield, and S. L. Bud'ko, Effect of pressure on the physical properties of the superconductor NiBi_3 , *J. Phys.: Condens. Matter* **31**, 035701 (2019).